THE EFFECT OF REALISTIC GEOLOGIC HETEROGENEITY ON LOCAL AND REGIONAL P/S AMPLITUDE RATIOS BASED ON NUMERICAL SIMULATIONS

Stephen C. Myers[1], Jeffery Wagoner[1], Leiph Preston[2], Ken Smith[2], Hrvoje Tkalcic[1], and Shawn Larsen[1]

Lawrence Livermore National Laboratory[1] and University of Nevada, Reno[2]

Sponsored by National Nuclear Security Administration
Office of Nonproliferation Research and Development
Office of Defense Nuclear Nonproliferation

Contract Nos. W-7405-ENG-48[1] and DE-FC03-02SF22656[2]

ABSTRACT

Generation of S-waves from explosion sources continues to be an intriguing area of seismological research. Empirical studies document a general decrease in regional S-phase amplitudes (compared to P phases) for explosions sources. Although the decrease in S-phase amplitude for explosive (compressional) sources is intuitive, a physical understanding of the dominant mechanism(s) that contribute to S-phase excitation does not currently exist. Despite the success of regional discriminant and magnitude methods that rely on decreased S-phase amplitude for explosion sources, instances remain – primarily in the ~1Hz band – where explosions produce anomalously large S-phase amplitudes that confound regional methods. In this study, we investigate the effect of realistic earth structure on the local and regional wavefield for explosive sources. We develop a detailed model of the Nevada Test Site (NTS) and southern Basin and Range, and simulate seismic propagation through the model using a full-elastic, finite-difference method. Our simulations are based on the Nonproliferation Experiment (NPE) explosion at the NTS, which was well recorded at permanent and temporary stations.

Much of our effort is devoted to construction of the earth model, translating the geologic model to seismic velocity, and validating seismic simulations. To construct the model we make use of the extensive geologic database covering the NTS as well as numerous published and unpublished geological and geophysical studies. The topographic representation for the NTS is based on a digital elevation model (DEM) with 10-meter resolution, and the southern Basin and Range DEM is 100-meter resolution. The geologic detail and accurate topography at the NTS provides a realistic rendition of the geologic structure near the NPE shot. We estimate seismic velocity in the upper crust by translating geologic units into either a constant velocity or – for units that span a significant depth range – a velocity/depth profile. Velocity structure of the lower crust and upper mantle, as well as crustal thickness, is adapted from published profiles in the southern Basin and Range. Validation of the velocity structure is accomplished by simulating both phase and amplitude characteristics of local and regional recordings of the NPE. Simulations and observed travel times are in excellent agreement for both P and S phases at local and regional distances. Local-distance simulations and observed seismograms, which tend to be less than one wavelength in distance from the source, are also in excellent agreement when an isotropic source is used and the model includes a topographic free surface. A Compensated Linear Vector Dipole (CLVD) source was also tested with poor results. At regional distance the first few swings of the simulated and observed Pn phase are in good agreement, but later swings do not necessarily agree in phase (dominant frequency ~1 Hz). However, the average amplitude of simulated and observed phases is in good agreement. Using this validated model we have conducted two tests to date: 1) regional simulations with a flat free surface and 2) simulations with an explosion event at mid crustal depth. Both simulations suggest that the topographic free surface has a strong effect on the production of regional S phases. With a flat free surface, the generation of regional S waves is significantly reduced; most of the converted energy is propagated into the mantle. For an explosion source at mid-crustal depth, appreciable S waves are not generated until the wavefield interacts with shallow structure and the free surface. The diminished amplitude of the P waves by the time they reach the free surface, and the reduced curvature of the wavefront, results in a significant reduction in the amplitude of converted S waves. While not conclusive our simulations to date suggest that near source complexity is a major contributor to the generation of S waves from explosions. In the case of the NPE, topography is the dominant scatterer.

OBJECTIVE

Regional monitoring relies heavily on comparisons of P- and S-phase amplitudes (Pomeroy et al., 1982; Walter et al., 1995). Further, widely used methods of determining magnitude make use of Lg and Lg coda amplitudes (e.g., Nuttli, 1986; Mayeda and Walter, 1996; Patton, 2001), and regional S-phases often add important arrival-time observations to limited, small-magnitude datasets used for location (Mayeda and Walter, 1996, Myers et al., 1999).

Most investigators agree that appreciable energy from the explosions is converted to S waves near the source, but the dominant P-to-S transfer mechanism is not agreed upon. Several physically reasonable transfer mechanisms are proposed, including P-to-S conversion at the free surface, spall, scattering of short-period surface waves, tectonic release, and rock-damage (e.g., Vogfjord, 1997; Day and Mclaughlin, 1991; Gupta et al., 1992; Wallace et al., 1985; Johnson and Sammis, 2001). Each mechanism fits a subset of observations, and each mechanism, with the exception of surface-wave scattering, is understood from first principles. Currently, the Rg-to-S mechanism is represented by an empirical transfer function (e.g. Gupta et al., 1992; Patton, 2001).

This project aims to study the physical process of near-source scattering to establish a fundamental understanding of this phenomenon. Our recent progress is in the areas of model construction, and pursuant numerical experiments on the effect of near-source topography, and event depth are presented below.

RESEARCH ACCOMPLISHED

In previous years of this project, we developed a detailed upper-crustal model centered on the 1993 NPE shot (Figure 1). The local model is 20 km on a side (including depth), and construction of the model leverages the extensive LLNL database of geological and geophysical information that includes mapping, bore-hole logs, seismic surveys, and gravity surveys (e.g. Healey et al. 1963). While much of LLNL geological database is unpublished, it constitutes a wealth of knowledge that was accumulated over decades of study at the NTS.

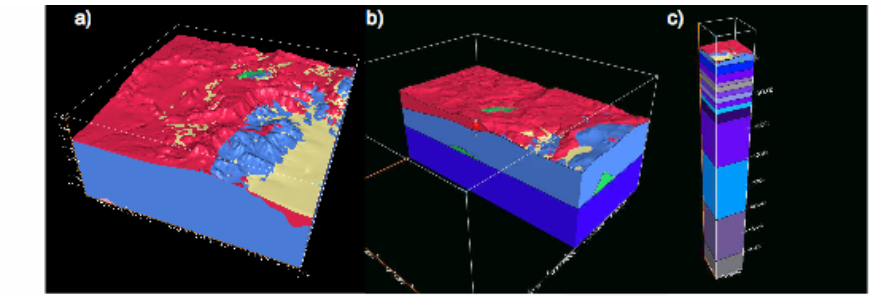

Figure 1. Local model around NPE shot determined from detailed geologic and geophysical studies. a) The entire local model. b) Cross section through the NPE shot. c) Local model merged into a lithospheric velocity stack.

The local model is imbedded in a regional model that extends to ~400 km from the NPE source (Figure 2). The default velocity structure is a one-dimensional model based on work of Patton and Taylor (1984). Deviation from the default model is based on published studies in the region. The current version of the model includes variations in upper-crustal structure based on regional geologic maps of Nevada, Utah, California, and Arizona. We assume that crystalline rocks are continuous into the lower crust, and that basin depths are proportional to the magnitude of local gravity anomalies (e.g., Blakely et al., 1997). The lower crustal velocities and Moho depth are modified based on the work of Zandt et al. (1995) and Mooney et al. (1998). Minor modifications to mantle velocities are based on refraction profiles summarized in Mooney et al. (1998). In specific areas we have incorporated tomographic studies, such as Biasi (2005) and Preston et al. (2005).

Considerable effort has been put into translating EarthVision models – as seen in Figures 1 and 2 – into seismic models. We have developed a suite of codes that translate geologic units into either a constant P wave, S wave, and density, or into a geologic unit may be translated into a specified portion of a velocity/depth profile. Generally, the upper crust is modeled as constant velocity units, such as sedimentary units and granite bodies. The lower crust and

upper mantle are modeled as smooth velocity vs. depth profiles, which are allowed to change laterally. Modeling the lower crust and upper mantle with smooth velocity profiles, as opposed to discrete layers, eliminates nuisance reflections and conversions from P to S energy.

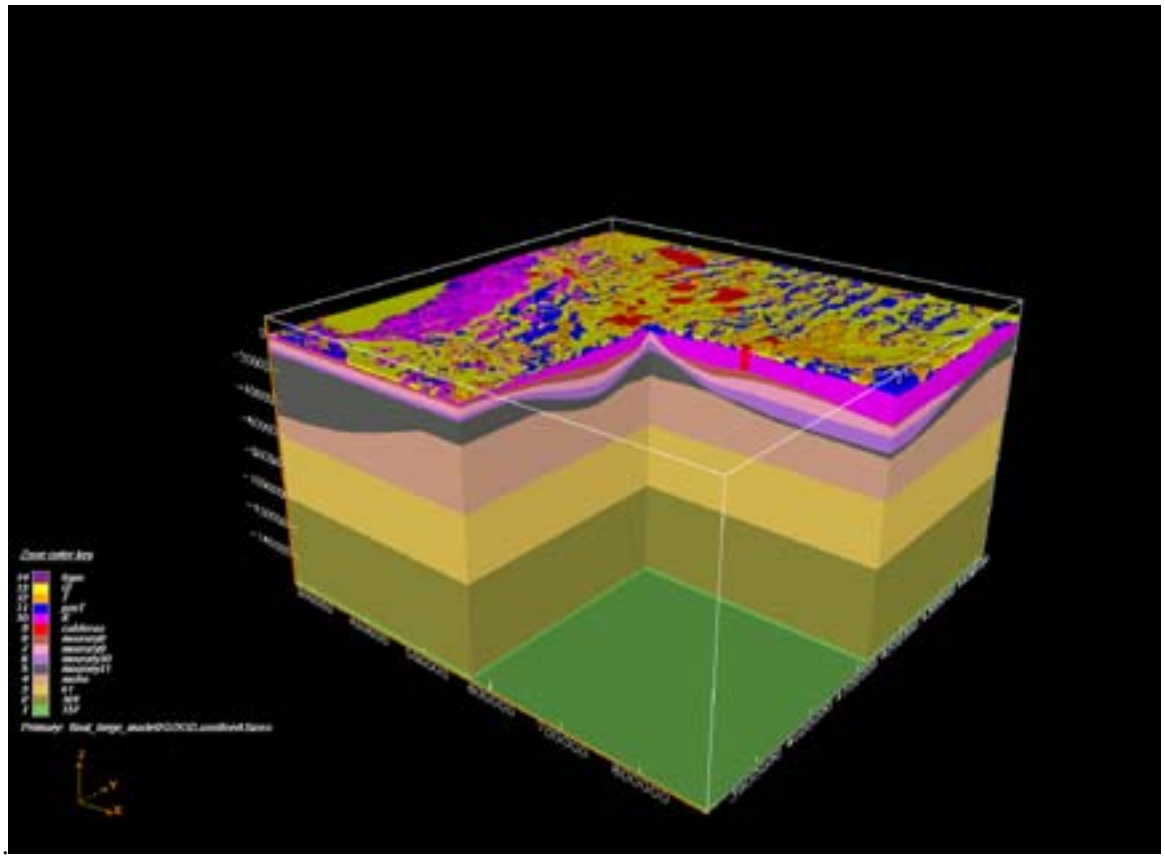

Figure 2. Regional geologic model centered on the Nevada Test Site. The model extends into California (to the left), Utah and Arizona (to the right). The model is a compilation of: geologic mapping; seismic profiles, receiver functions, and tomography; gravity modeling for basin structure.

Model Validation using NPE Observations

We use the E3D code of Larsen and Grieger (1998) for seismic simulations. E3D is a full elastic code that allows the input of a general geologic structure, including the free surfaces. All of our simulations use a grid spacing of 60 m, which enables interpretation to 3 or 4 Hz.

Our numerical simulations are based on the 1993 NPE. The NPE was a 1-kiloton chemical explosion at the NTS. NPE details and research reports can be found in Denny and Stull (1994). Figure 3 shows the extensive network of stations that recorded the NPE. We have compiled all these recordings to validate our model. We begin with the local recordings, which we used both to validate the near-source model and to estimate the NPE moment tensor.

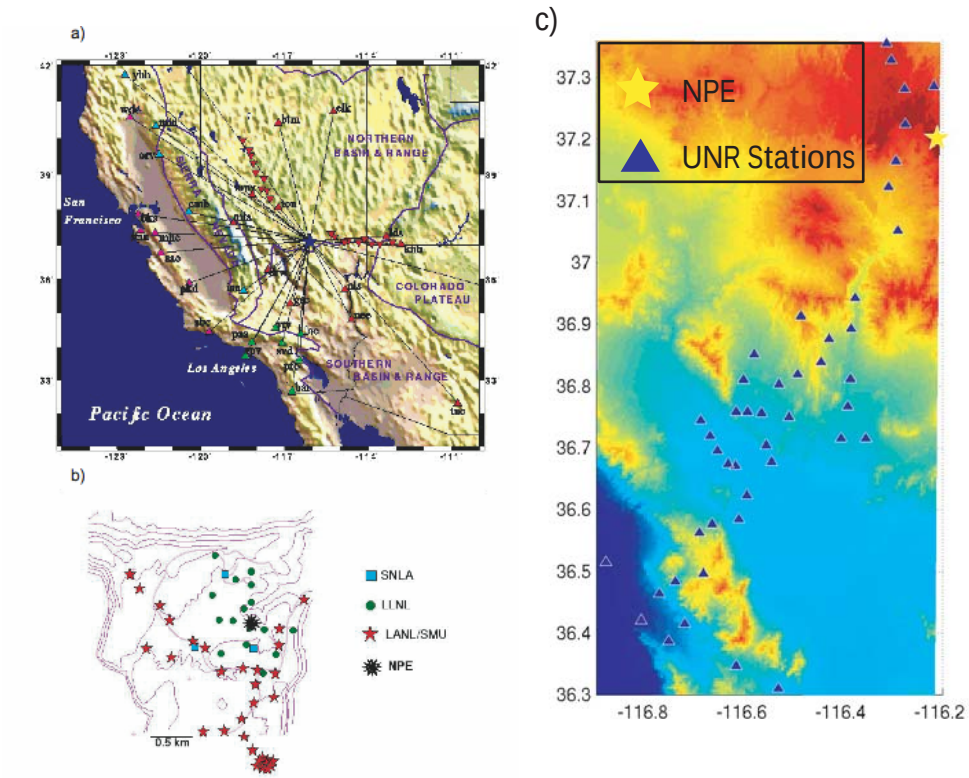

Figure 3. Stations with recordings of the NPE shot. We have compiled waveforms from all of these stations.

Figure 4 shows an example waveform (black) from a station that is approximately 2 km from the NPE. Simulations (red) with combinations of isotropic (Figure 4 a,b) and CLVD (Figure 4 c,d) moment tensors and topographic free surface (Figure 4 a,c) and flat free surface (Figure 4 b,d) are compared with the data. It is clear that the isotropic source in a model that includes the topographic free surface is the best fit to the data. Comparisons with other local data (not shown) are similar, and we conclude that the NPE is best modeled as an isotropic source.

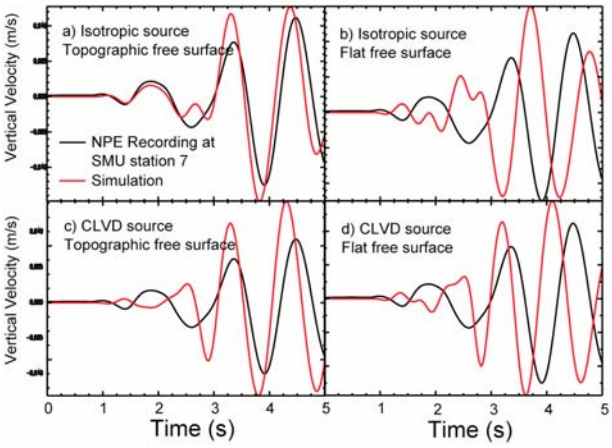

Figure 4. Recorded (black) and simulated (red) displacement seismograms for the NPE shot. These 3-dimensional simulations make use of the local NPE model (see above). Event-station distance is approximately 2 km. a) Simulation with isotropic moment tensor and free surface based on DEM. b) Simulation with isotropic source and flat free surface. c) Simulation with CLVD moment tensor with DEM free surface. d) Simulation with CLVD moment tensor and flat free surface. The NPE is best modeled as an isotropic source. Simulation with a realistic free surface is essential to match the data.

Figure 5 is an example of our regional validation effort. In this example we use the temporary, broadband (STS-2 sensor) deployment fielded by the University of Arizona. The cross section is color coded to P-wave velocity, which was taken from our regional 3-dimensional model. The upper crust is characterized by Paleozoic sedimentary rocks, which are interrupted by low-velocity basins. Velocity in the mid- and lower crust primarily increases with depth, but we include minor lateral variation in velocity as well as changes in Moho depth based on the work of Zandt et al. (1995). The interface between light and dark red in the lower quarter of the cross section is the Moho. We have superimposed a snap shot of the seismic wavefield on the cross section to demonstrate the complexity that results from this relatively simple model.

The traces shown in Figure 5 compare recorded (black) and synthetic (red) velocity seismograms. Both velocity and synthetic records are band passed between 0.7 Hz and 3 Hz. Amplitudes are normalized because geometric spreading in the 2-dimensional synthetics is incorrect. In general, the comparison of observed and synthetic data is favorable. The degree of waveform complexity is nearly identical, and it would be difficult to tell which trace is real based on simple inspection. The relative amplitudes of the real and synthetic waveforms are also in good agreement (with the notable exception of station 8, where synthetic amplitudes after the first arrival are too large). Although the phase is matched in many instances (particularly the first arrival), we cannot claim to have simulated phase reliably. Nonetheless, the overall agreement between observed and synthetic data is very good, especially considering that the model was not directly derived from the data. Figure 5b shows cumulative energy for the 6 recordings and synthetics. In most cases, the cumulative energy curves of data and synthetics are in good agreement. We also note that synthetic estimates are high in some case and low in others, i.e., there is not a consistent bias across all stations. We find that the overall model performance is good and that variability can be attributed to station site effects.

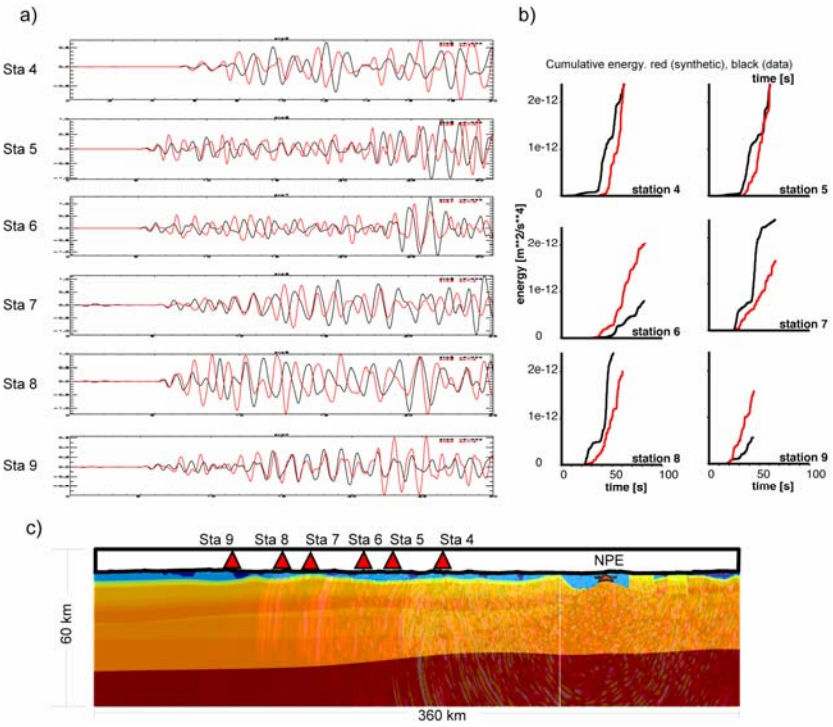

Figure 5. Model validation with regional seismic simulations of the U. Arizona broadband deployment (line extending east from NPE in Figure 2). a) Vertical velocity recordings of the NPE between 0.7 Hz and 3 Hz (black) with synthetics (red) for comparison. Amplitudes are normalized. A separate 2-dimensional simulation was made for each of the stations to account for slight azimuth variations in structure. The general character of the observed seismograms is matched by the synthetics, suggesting that the regional model is a good representation of true structure. b) Cumulative energy for observed and synthetic waveforms in a). c) Cross-section shows a snap shot of the seismic wavefield overlain on a P-wave velocity for the station 9 simulation; west is to the right. The transition from red to near black in the lower quarter of the cross section is the Moho.

Observed and synthetic P/S ratios are in good (but not perfect) agreement (Figure 6). In a band pass of 0.5 Hz to 1.0 Hz the data are biased towards higher P/S ratios. We are currently working to understand the bias, but we note that the bias is only a couple tenths, which is well within the spread of most empirical P/S plots. In the 1.0 Hz to 3.0 Hz band, P/S ratios for both data and synthetics increase, suggesting that our model is characterizing the wavefield at these frequencies.

Table 1: P/S ratio for data and synthetics

	0.5 to 1.0 Hz		1.0 to 3.0 Hz	
	data	synth	data	synth
sta4	0.504	0.143	1.568	0.374
sta5	0.592	0.200	0.551	0.601
sta6	0.153	0.230	0.336	0.424
sta7	0.724	0.518	0.860	1.290
sta8	1.032	0.406	1.665	0.469
sta9	0.741	0.480	0.934	0.802

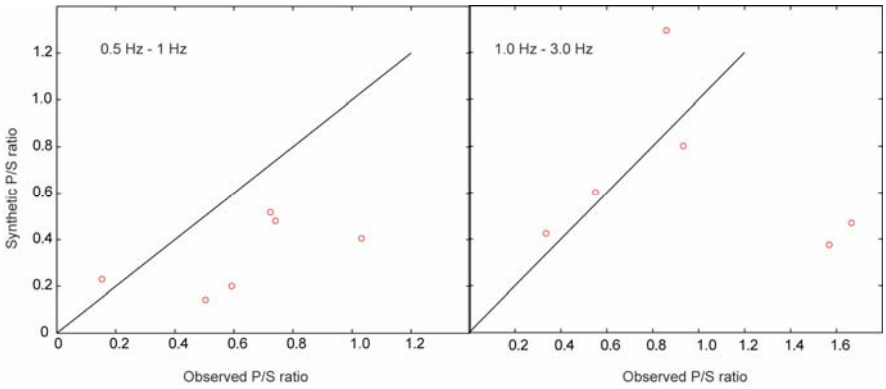

Figure 6: Comparison of observed and synthetic P/S ratios.

The Effect of Topography on P/S Ratios

Figure 7 is a map-view snap shot of a local simulation with and without topography (note that these are the same simulations that produced the synthetic seismograms in Figure 4 a,b). The topographic level at the NPE epicenter is applied uniformly in the flat free surface simulation with surface velocities filled to the flat free surface or with truncation of the structure (depending on whether the elevation is lower or higher than at the NPE). Figure 7 shows that local topography immediately imparts disorder (scattering) into the wavefield.

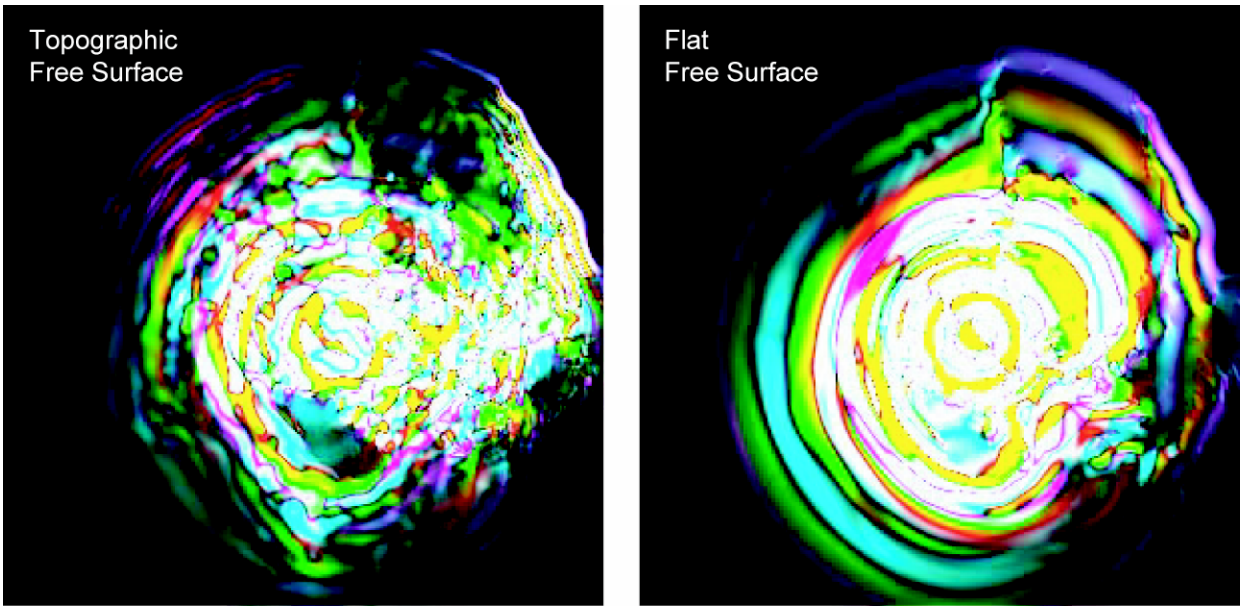

Figure 7. Map view of simulations with topographic free surface based on a digital elevation model (left) and flat free surface (right). Red, magenta and blue colors are P-waves. Green and yellow colors are S-waves. The map views shown above are 20 km on a side. Images are snap shots at approximately 5.5 seconds after event origin time and are at the lowest topographic elevation in the model. Detailed geologic structure from local mapping and geophysical studies is included in both simulations. Inclusion of realistic topography complicates the wave field considerably with appreciably more scattering.

Figure 8 shows synthetic spectra and seismograms of P-potential and S-potential at approximately 5 km from the source (taken from the simulations shown in Figure 7). In all cases, the S-potential exceeds the P-potential, which is presumably the result of free surface effects. However, the real topographic free surface results in a frequency-dependent P/S ratio. In fact, the P/S ratio is significantly decreased at frequencies close to 1 Hz. Although these results are preliminary, the qualitative similarities in the frequency dependence of observed P/S ratios (mentioned in the Objectives section) and the synthetic P/S ratios for simulations that include real topography is suggestive. Further testing and rigor will determine whether topographic scattering is the primary mechanism for S waves in the 1 Hz band.

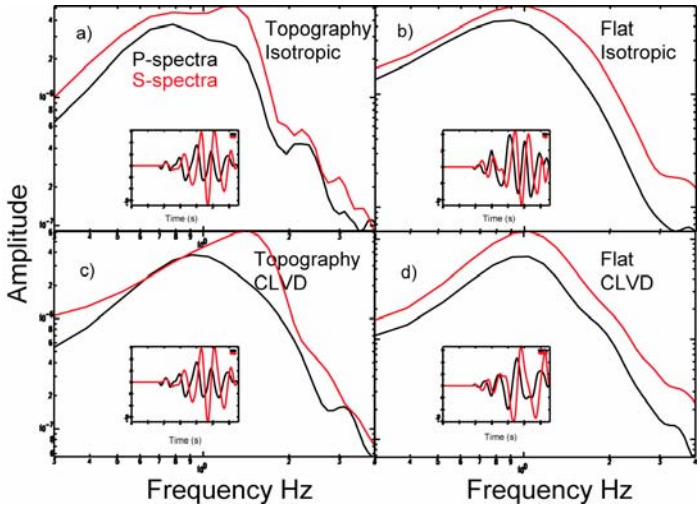

Figure 8. P (black) and S (red) displacement spectra and seismograms for simulations of the NPE shot (Simulations shown in Figure 7). These 3-dimensional simulations make use of the local NPE model (see above). The inset seismograms are P-potential (black) and S-potential (red) for a location approximately 5 km from the source. The spectra are derived from P and S potential seismograms. a) Simulation with isotropic moment tensor and free surface based on digital elevation model (DEM). b) Simulation with isotropic source and flat free surface. c) Simulation with compensated linear vector dipole (CLVD) moment tensor with DEM free surface. d) Simulation with CLVD moment tensor and flat free surface. Both isotropic and CLVD moment tensors produce a distinctly frequency-dependent P/S ratio.

The Effect of Source Depth on P/S Ratios

Results presented above suggest that near-source scattering, particularly scattering off of the free surface, boosts the amplitude of radiated S waves at the expense of P-wave amplitudes. We test this hypothesis by comparing the simulation of a shallow source with a simulation of a deep (mid crustal) source (Figure 9). Near-source heterogeneity for the shallow source (upper-crustal structure and topography) is considerable. Near-source heterogeneity for the deep source, where velocity is changing smoothly with depth, is minor. In both instances the source is isotropic (explosion) with the same moment. The model is approximately 300 km wide and 150 km deep. Some artifacts from reflections off of the side of the model are evident, but these artifacts do not muddle the overall picture.

The difference between the shallow- and deep-source simulations is striking. For the shallow source, S waves grow to large amplitudes within seconds. The large S waves radiate from the source in all directions. Therefore, S-waves are observed to propagate at steep angles into the mantle (and could propagate to teleseismic distances), as well as at shallow angles into the crustal waveguide to regional distances. For the deep source, S waves are all but absent until the P-wave enters the upper crust. Notable conversion to S-waves does occur, but the S-wave amplitudes are significantly smaller than they are for the shallow source. Much of the S-wave energy is trapped in the upper crust, forming a P-coda. S energy that escapes local, upper-crustal structures (e.g., basins) is reflected downward at steep angles. Therefore, the majority of the S energy that escapes the upper crust is transmitted into the mantle, and little energy is trapped in the crustal waveguide.

CONCLUSIONS AND RECOMMENDATIONS

We have constructed a regional model centered on the NTS based on published and unpublished studies. The starting point of the regional model is a 1-dimensional model that is based on surface-wave studies. We include significant 3-dimensional modifications to the 1-dimensional model based on receiver function, refraction, reflection, and gravity studies. The regional model includes a detailed upper crustal model centered on the NPE explosion. This local model is constrained by geologic maps, borehole data, and geophysical studies at the NTS. The local model is seamlessly imbedded into a regional model to enable realistic simulations of NTS sources to regional distance.

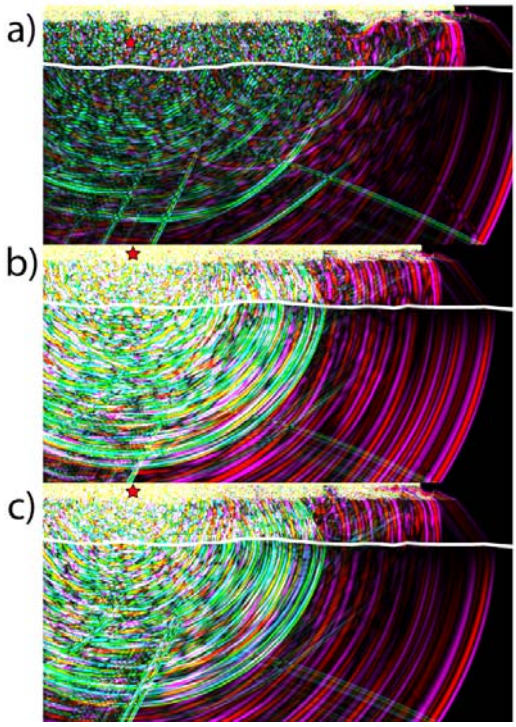

Figure 9. Regional, 2-dimensional simulation showing the difference between a) mid-crustal source, b) shallow source with complex geology and flat topography, and c) shallow source with complex geology and topographic free surface. In each case the source is isotropic. The model is approximately 300 km wide and 150 km deep. Snap shots are at approximately 75 seconds after the source origin time. P waves are red, and S waves are green and yellow. The shallow sources generate vastly more S waves (green and yellow) than the deeper source. The intensity of Pg (red and blue crustal phase on the right side of each panel) is greater for the deeper source.

Validation of the model is based on recordings and simulations of the NPE shot, as well as phase travel-times from NTS explosions. Validation of the local model is complete and the model reliably predicts local NPE waveforms. Validation of the regional model is on-going. Although we do not predict regional waveforms above ~1Hz, arrival times and relative amplitudes of regional phases are reliably predicted.

Local 3-dimensional simulations demonstrate that topographic scattering is an important source of S-wave generation for the NPE. We find that topographic scattering peaks S-wave amplitudes at approximately 1 Hz, which is in agreement with observations in many instances (at NTS and other locales). Topographic scattering produces a disordered wavefield and scatters energy in all directions. Simulations with a flat free surface produce S waves, but little frequency dependence is observed.

Regional simulations demonstrate that a shallow NPE source produces appreciable S waves that radiate at a large range of ray parameters. For shallow sources, S waves generated through structural and topographic scattering propagate in all directions. This means that the S waves propagate at steep angles into the mantle (and would presumably continue to teleseismic distance) as well as into the regional waveguide to form Sn and/or Lg. Our results are consistent with those of similar numerical studies (e.g., Xie et al., 2005). When the equivalent NPE source is placed in the mid crust, S-wave generation is significantly diminished. S waves are generated as the P wave traverses the upper crust and reflects off of the topographic free surface, but S waves that escape the upper crust travel at steep angles and are largely transmitted into the mantle.

ACKNOWLEDGEMENTS

We acknowledge the LLNL containment program for generous access to their extensive database of geologic and geophysical studies at the NTS. We also would like to than Glenn Biasi and Walter Mooney for providing regional geophysical information.

REFERENCES

Blakely, R. J., R. C. Jachens, J. P. Calzia, and V. E. Langenheim (1997). Cenozoic basins of the Death Valley extended terrane as reflected in regional-scale gravity anomalies, L.A. Wright and B.W. Troxel, eds., Cenozoic Basins of the Death Valley Region: Boulder, CO, *Geol. Soc. Am. Special Paper 333*.

Biasi, G. (2005). Mantle lithospheric clues to Walker Lane evolution, presented at the 2005 SSA meeting, Incline, NV.

Day, S., and K. Mclaughlin (1991). Seismic source representations for spall, *Bull. Seismol. Soc. Am*. 81: 191–201.

Denny, M. D., S. P. Stull (1994). Proceedings of the Symposium on the Non-Proliferation Experiment (NPE): Results and Implications for Test Ban Treaties, Rockville Maryland; Lawrence Livermore National Laboratory.

Gupta, I. N., W. W. Chan, and R. A. Wagner (1992). A comparison of regional phases from underground nuclear explosions at East Kazakh and Nevada Test Sites, *Bull. Seismol. Soc. Am*. 82: 352–382.

Healey, D. L. and Miller, C. H. (1963). Gravity survey of the Gold Meadows Stock, Nevada Test Site, Nye County, Nevada. *USGS Technical Letter NTS-40*.

Johnson, L.R., and C.G. Sammis (2001). Effects of rock damage on seismic waves generated by explosions, *Pageoph*, 158, 1869–1908.

Larsen, S., and J. Grieger (1998). Elastic modeling initiative, Part III: 3-D computational modeling, in *Soc. Expl. Geophys. Conference Proceedings*, 6: 1803–1806.

Mayeda, K., and W. Walter (1996). Moment, energy, stress drop, and source spectra of western United States earthquakes from regional coda envelopes, *Jour. Geophys. Res*. 101: 11,195–11,208.

Myers, S.C., W.R. Walter, K. Mayeda, L. Glenn (1999). Observations in support of Rg scattering as a source for explosion S waves: regional and local recordings of the 1997 Kazakhstan depth of burial experiment, *Bull. Seismol. Soc. Am*. 89: 544–549.

Mooney, W., G. Laske, G. Masters (1998). Crust 5.1: a global crustal model at 5x5 degrees, *Jour. Geophys. Res*. 103: 727–747.

Nuttli, O. W. (1986). Yield estimates of Nevada Test Site explosions obtained from seismic Lg waves, *J. Geophys. Res*. 91: 2137–2151.

Patton, H. J. and S. R. Taylor (1984). Q-structure of the basin and range from surface waves, *Jour. Geophys. Res*. 89: (NB8) 6929–6940.

Patton, H. J. (2001). Regional magnitude scaling, tranportability, and Ms:mb discrimination at small magnitudes, *Pageoph* 158: 1951–2015.

Pomeroy, P., W. Best, and T. McEvilly (1982). Test ban treaty verification with regional data - a review, *Bull. Seismol. Soc. Am*. 72: S89-S129.

Preston, L., K. Smith, and D. vonSeggern (2005). 3D velocity structure of the Yucca Mountain, *Seismo. Soc. Am. Spring meeting*, presented at the 2005 SSA meeting, Incline, NV .

Vogfjord, K. (1997). Effect of explosion depth and earth structure on the excitation of Lg waves: S* revisited, *Bull. Seismol. Soc. Am*. 87: 1100–1114.

Wallace, T., D. Helmberger, and G. Engen (1985). Evidence for tectonic release from underground nuclear explosions in long period S waves, *Bull. Seismol. Soc. Am*. 75: 157–174.

Walter, W., K, Mayeda, and H. Patton (1995). Phase and spectral ratio discrimination between NTS earthquakes and explosions: Part I: empirical observations, *Bull. Seismol. Soc. Am*. 85: 1050–1067.

Xie, X. B., Z. Ge, T. Lay, Investigating Explosion source energy partitioning and Lg-wave excitation using a finite-difference plus slowness analysis method, Bull. Seism. Soc. Am., 95, 2412-2427, 2005.

Zandt, G. SC Myers, TC Wallace (1995). Curst and mantle structure across the Basin and Range – Colorado plateau at 37° north latitude and implications for Cenozoic extension mechanism, *Jour. Geophys. Res*. 100: 10,592–10,548.